Nanoscale

Check for updates

Single atom detachment from Cu clusters, and diffusion and trapping on CeO₂(111): implications in Ostwald ripening and atomic redispersion†

Qiang Wan,[a] Fenfei Wei,[a] Yingqi Wang,[b] Feiteng Wang,[c] Linsen Zhou,[b] Sen Lin, ID *[a,b] Daiqian Xie ID *[c] and Hua Guo ID *[b]

Ostwald ripening is a key mechanism for sintering of highly dispersed metal nanoparticles in supported catalysts. However, our microscopic understanding of such processes is still primitive. In this work, the atomistic mechanism of the Ostwald ripening of Cu on CeO₂(111) is examined *via* density functional theory calculations. In particular, the detachment of a single Cu atom from ceria supported Cu_n (n = 2–10, 12, 14, 16, 18, and 20) clusters and trapping on the CeO₂(111) surface is investigated in the absence and presence of CO adsorption. It is shown that the adsorption of CO on Cu reduces its detachment energy, which helps in the formation of single atom species on CeO₂(111). In addition, the Cu_1–CO species is found to diffuse on the CeO₂(111) surface with a much lower barrier than a Cu atom. These observations suggest an efficient mechanism for the Ostwald ripening of Cu clusters supported on ceria in the presence of CO. It is further predicted that the Cu_1–CO species can eventually migrate to a step site on ceria, generating a stable single-atom motif with a relatively larger binding energy. Finally, the single Cu atom catalyst is shown to possess high activity for the oxygen reduction reaction.

1. Introduction

Metal oxide supported copper nanoparticles (NPs) are widely used as catalysts for a variety of heterogeneous reactions such as methanol synthesis, methanol steam reforming, the water gas shift (WGS) reaction, and CO oxidation.[1–8] While the copper NPs are well established as the active phase of the catalysts, their properties are significantly influenced by the nature of the metal oxide support, which not only provides the dispersion medium but also affects both the physical and chemical properties of the metal NPs.[9,10] Despite high catalytic performance, the supported Cu NPs commonly experience sintering under high-temperature reaction conditions, resulting in partial or complete loss of the expected catalytic activity.[11–13] Such sintering processes manifest as growth of NP sizes at the expense of smaller NPs, which reduces the surface area of the

active phase and thus the number of active sites. Finding ways to prevent and minimize sintering is an important but unsolved problem in heterogeneous catalysis.[14,15]

It is well established that the sintering of supported metal NPs can take place following either the Ostwald or Smoluchowski ripening pathway.[16,17] The former mechanism, which is also called atomic ripening, is thought to involve the detachment of atomic metal species from a small metal NP followed by migration and attachment to another larger NP, while the latter, also known as particle migration and coalescence, involves NP migration on the surface and merging with other NPs. Both mechanisms are driven by thermodynamics, but kinetics depends on several factors, such as the NP size and shape as well as its interaction with the substrate.[18–20] Extensive experimental evidence has suggested that the former is often the main mechanism for small NPs.[17,21] However, the detachment of a single atom from metal NPs is often thermodynamically unfavoured mainly due to the high cohesive energy of metal NPs. As a result, direct formation of single metal species that are mobile on the oxide support requires an unrealistically high temperature. Interestingly, common adsorbates, such as CO, have been found to play an important role in the sintering of metal NPs on oxide surfaces,[22–27] presumably by weakening the metal–metal bonding in the adsorbed NPs. For example, a recent study by Ouyang, Liu and Li convincingly established that carbonyl complexes with single Rh

[a]State Key Laboratory of Photocatalysis on Energy and Environment, College of Chemistry, Fuzhou University, Fuzhou 350002, China. E-mail: slin@fzu.edu.cn
[b]Department of Chemistry and Chemical Biology, University of New Mexico, Albuquerque, New Mexico 87131, USA. E-mail: hguo@unm.edu
[c]Institute of Theoretical and Computational Chemistry, Key Laboratory of Mesoscopic Chemistry, School of Chemistry and Chemical Engineering, Nanjing University, Nanjing 210023, China. E-mail: dqxie@nju.edu.cn
†Electronic supplementary information (ESI) available. See DOI: 10.1039/c8nr06232c

atoms, rather than bare metal atoms, are the mobile species in CO-assisted Ostwald ripening of Rh clusters on a TiO_2 surface.[28] The importance of the mobile adsorbate–metal species in Ostwald ripening has been demonstrated in several other theoretical studies.[29–35]

Among the metal oxides used as supports, CeO_2 has recently attracted considerable attention because of its unusual sinter resistance and high oxygen mobility.[36] Recent work has revealed that this oxide is unique in trapping single metal atoms in preparing single-atom catalysts (SACs),[37–43] a new frontier in heterogeneous catalysis.[44] The atomically dispersed metal atoms on CeO_2 have unique chemical and physical properties, usually different from those of supported NPs. For example, Qiao et al. found that CeO_2-supported Au single atoms are highly active for CO oxidation at a temperature of ~80 °C.[38] Dvořák et al. pointed out the importance of step edges in the formation of SACs on ceria.[41] Datye and co-workers reported that Pt could be atomically dispersed on ceria and exhibits high reaction activity towards CO oxidation.[39,43] The first-principles studies of such systems have shed valuable light on the mechanisms of these SACs.[30,32,45–47] The formation of SACs usually requires mobile single-atom species on the oxide surface, and this atomic redispersion is thus related to Ostwald ripening. To understand the formation of SACs, density functional theory (DFT) and ab initio molecular dynamics (AIMD) have been used by Li and co-workers to gain insight into the stability and dynamics of single atom species, using Au on $CeO_2(111)$ as a prototype.[30] These studies revealed, among other things, that CO can significantly promote the disintegration of Au NPs through the formation of an adsorbed Au_1–CO complex.

Despite extensive experimental and theoretical efforts, the mechanism of Ostwald ripening of other metal NPs on ceria is still unclear because of the complexity of ceria supports and the challenges of in situ characterization. In this work, we investigate the atomistic mechanism for Cu detachment and migration on CeO_2 surfaces using a first principles method. Such systems having practical relevance as Cu catalysts supported by ceria are known to exhibit specific reaction activity towards several important industrial processes such as the WGS reaction and methanol synthesis. For example, Wang et al. demonstrated recently that single-atomic Cu substituted CeO_2 can optimize the CO_2 electrocatalytic reduction to CH_4 with a faradaic efficiency as high as 58%, highlighting the potential catalytic application of the Cu SAC.[48] The Cu/CeO_2 system also serves as a prototype for understanding microscopic mechanisms in Ostwald ripening. It is particularly interesting to compare this system to Au NPs supported on ceria since the cohesive energy of Cu (3.48 eV) is comparable to that of Au (3.81 eV). Specifically, in this work, the stability of single Cu atoms and Cu_n clusters (n = 2–10, 12, 14, 16, 18, and 20) and the migration of species containing a single Cu atom on $CeO_2(111)$ and CeO_2 steps are investigated by DFT. The influence of CO on the sintering process is highlighted and the implications in the Ostwald ripening of supported Cu NPs are discussed. Finally, we explore the formation of a possible Cu/CeO_2 SAC as a result of the atomic redispersion on the ceria surface and a potential application of this SAC.

2. Computational methods

All the spin-polarized DFT calculations were performed using the generalized gradient approximation (GGA) with the PW91 exchange–correlation functional[49] as implemented in the VASP code.[50–52] The electronic wave functions were expanded in plane waves up to a cutoff energy of 400 eV and the ionic core electrons were approximated by the projector augmented-wave (PAW) method.[53] Since the standard GGA functional fails to accurately describe the highly localized Ce 4f-orbitals, a Hubbard-like term is added in the so-called DFT+U treatment with U = 4.5 eV applied to the Ce 4f states.[54]

The 111 facet of CeO_2 is the most stable surface and thus chosen in our study to gain insight into the sintering of Cu NPs. Cu clusters supported by $CeO_2(111)$ were modelled using a periodic slab with a unit cell of a = 13.33 Å and b = 15.39 Å including 32 Ce and 64 O atoms, in which six atomic (Ce and O) layers with top three atomic layers and the adsorbates were fully relaxed while the other atoms were fixed. A 1 × 1 × 1 k-point mesh was adopted to sample the Brillouin zone, which was shown to be converged. Isolated Cu_n clusters with n equal to 2–10, 12, 14, 16, 18, and 20 were optimized in a periodic box with the same size. Although the metal clusters are much smaller than typical NPs on real catalysts, they are chosen in our studies because of computational constraints. They should nonetheless provide insights into the relevant energetics of the key steps in Ostwald ripening.

For the migration of the atomic Cu species on $CeO_2(111)$ with or without the CO adsorbate, a smaller unit cell of 7.65 × 13.25 Å^2 with 16 Ce and 32 O atoms was adopted with top three atomic layers, and the adsorbates were allowed to relax while bottom three atomic layers were fixed. The k-point mesh was set to 2 × 2 × 1.

For the CeO_2 step surface, a low-energy monolayer-high step was created by removing a large portion of the top layer. This slab model has the edge of the step oriented along the [1$\bar{1}$0] direction and contains a total of nine atomic layers, similar to models used in previous reports.[41] This unit cell contained 40 Ce and 20 O atoms with the bottom three layer atoms fixed in their bulk positions. A 2 × 1 × 1 k-point mesh was adopted to sample the Brillouin zone. A vacuum space larger than 14 Å was employed between the neighbouring interleaved slabs for all the surface models.

The overall binding strength of Cu in Cu_n clusters is characterized using the cohesive energy (E_{coh}), which is defined below for gas-phase Cu_n clusters:[34]

$$E_{coh} = [nE(Cu) - E(Cu_n)]/n \qquad (1)$$

where $E(Cu)$ and $E(Cu_n)$ represent the calculated energies of an isolated Cu atom and the isolated Cu_n cluster, respectively.

For Cu_n clusters supported on $CeO_2(111)$, the E_{coh} can be computed as:

$$E_{coh} = [nE(Cu) + E(CeO_2) - E(Cu_n/CeO_2)]/n \qquad (2)$$

where $E(CeO_2)$ and $E(Cu_n/CeO_2)$ represent the calculated energies of the bare $CeO_2(111)$ surface and the $CeO_2(111)$ supported Cu_n cluster, respectively.

To understand the energy costs for detaching a single Cu atom from a cluster to the most stable oxygen hollow site on the ceria surface, the detachment energy (E_{det}) is defined as follows:

$$E_{det} = E(Cu_{n-1}/CeO_2) + E(Cu/CeO_2) - E(Cu_n/CeO_2) \\ - E(CeO_2) \qquad (3)$$

where $E(Cu_{n-1}/CeO_2)$ and $E(Cu/CeO_2)$ represent the calculated energies of the $CeO_2(111)$ supported Cu_{n-1} clusters and Cu_1 atom, respectively.

Similarly, the detachment energy for removing one Cu_1-CO complex from a CO decorated Cu cluster to the most stable oxygen site ($E_{det}(CO)$) is given below:

$$E_{det}(CO) = E(Cu_{n-1}/CeO_2) + E(Cu_1-CO/CeO_2) \\ - E(Cu_n-CO/CeO_2) - E(CeO_2) \qquad (4)$$

where $E(Cu_1-CO/CeO_2)$ and $E(Cu_n-CO/CeO_2)$ represent the calculated energies of the $CeO_2(111)$ supported Cu_1-CO complex and the supported Cu_n clusters with a CO molecule adsorption at an arbitrarily selected corner Cu atom, respectively.

The binding energies for Cu_n on $CeO_2(111)$ are calculated from the following equation:

$$E_b = E(Cu_n/CeO_2) - E(Cu_n) - E(CeO_2) \qquad (5)$$

where $E(Cu_n/CeO_2)$, $E(Cu_n)$ and $E(CeO_2)$ represent the calculated energies of Cu_n supported on CeO_2, free Cu_n, and CeO_2, respectively.

The climbing image-nudged elastic band (CI-NEB)[55,56] approach was employed to simulate the diffusion of a single Cu atom or the Cu_1-CO complex on $CeO_2(111)$. The activation barrier for diffusion was calculated as the energy difference between the transition state and the initial state while the reaction energy for each reaction step was calculated from the energy difference between the final state and the initial state. The total energy converges to less than 10^{-4} eV and the convergence of relaxation was checked with the 0.05 eV $Å^{-1}$ criterion.

3. Results and discussion

3.1 Stability and disintegration of Cu clusters on $CeO_2(111)$

We first assess the cohesive energy for isolated Cu clusters with different sizes, which gives an indication of the average Cu–Cu bond strength. To this end, we choose the stable structures of Cu_n (n = 2–10, 12, 14, 16, 18, and 20) clusters in isolation (Fig. 1(a)), including two-dimensional (2D) and three-dimensional (3D) clusters determined in previous reports.[57-63]

The cohesive energy for Cu clusters with different sizes is calculated and displayed in Fig. 2. It can be seen that the cohesive energy increases significantly with the increasing Cu cluster size from n = 2 (1.12 eV) to 8 (2.14 eV). For larger clusters with sizes between 9 and 20 atoms, the increment of cohesive energies becomes smaller. Extrapolation to a large n (larger Cu_n clusters with n = 35, 55, 100 and 230 are included) leads to an estimate of the copper bulk E_{coh} equal to 3.69 eV, in good agreement with the experimental value of 3.48 eV (ref. 64) (see Fig. S1 and S2† for details). These results clearly demonstrated that the Cu–Cu bonding in isolated Cu clusters is strong, and the detachment of a single Cu atom from the clusters is expected to be energetically costly.

Since the Cu atoms are oxyphilic, the gas phase clusters are placed over $CeO_2(111)$ in such a way as to maximize their interaction with the oxygen atoms on the surface. These structures are then optimized, and their geometries are illustrated in Fig. 1(b). It can be seen that the shapes of all the clusters are not significantly changed upon adsorption, although the Cu–Cu bond lengths of the interfacial layer typically become longer. For example, the Cu_{10} cluster still assumes a three-layer structure, but the average Cu–Cu distance in the bottom layers, which is interfaced with the $CeO_2(111)$ surface, elongated from 2.45 to 2.67 Å upon adsorption.

The binding energies for these Cu clusters on $CeO_2(111)$ are calculated to be $-2.02 - -6.72$ eV (Table S1†), indicating that they are strongly bonded to ceria. We also tested the impact of defect sites on the adsorption of Cu clusters on $CeO_2(111)$. For example, Cu_8 adsorption was studied on the $CeO_2(111)$ surface with an oxygen vacancy and the calculated binding energy of Cu_8 is -3.71 eV, much smaller than that (-4.44 eV) without any oxygen vacancy. It is thus unlikely for Cu_8 to adsorb on the oxygen vacancy of CeO_2. Therefore, the oxygen vacancy was not considered in the following sections. As a reference, the binding energy of a single Cu atom adsorbed at the most stable oxygen hollow site is -2.55 eV, which is much smaller than the cohesive energy of bulk Cu. The cohesive energies for the supported Cu clusters are compared with those in the gas phase in Fig. 2. It is apparent from the figure that the ceria support, through the formation of Cu–O bonds, leads to higher cohesive energies than those in the gas-phase. In other words, the gap between the two cases is largely due to the binding energy of the cluster on $CeO_2(111)$. Similar results were found for Pd clusters on CeO_2 as substantially higher cohesive energies were obtained, again suggesting the role of the ceria support in stabilizing the clusters.[34] The largest difference of 1.44 eV is found for Cu_3. However, such a difference becomes smaller with an average value of 0.33 eV when the clusters have 14–20 atoms.

Now we consider the energy cost for detaching a single Cu atom from the Cu clusters on $CeO_2(111)$. Fig. 3 shows the detachment energy for removing a Cu atom from Cu_n clusters adsorbed on the $CeO_2(111)$ surface and placing it on the most stable oxygen hollow site on $CeO_2(111)$. It is clear from the figure that the detachment is an endothermic process for most Cu clusters on $CeO_2(111)$. There is also a clear size effect for
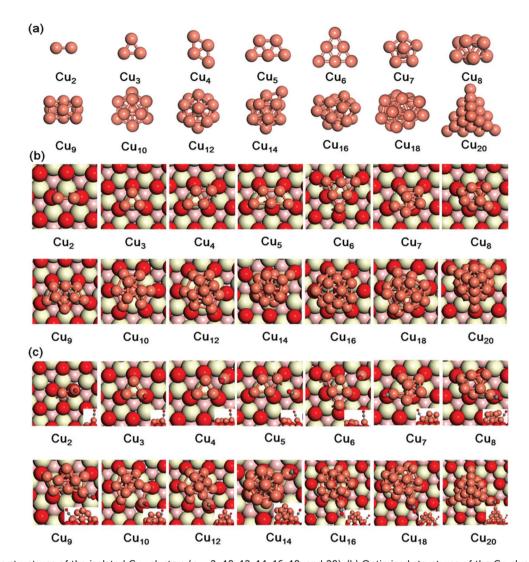
Fig. 1 (a) Stable structures of the isolated Cu_n clusters (n = 2–10, 12, 14, 16, 18, and 20). (b) Optimized structures of the Cu clusters on $CeO_2(111)$ and (c) optimized structures of CO adsorption on the corner Cu atom of Cu clusters on $CeO_2(111)$. Color scheme: Ce, yellow; surface O, red; subsurface O, coral; Cu, bronze; C, grey.
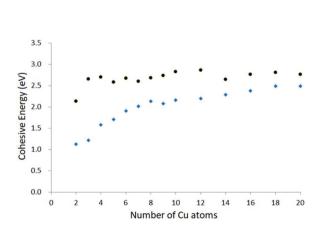

Fig. 2 Calculated cohesive energies of $CeO_2(111)$ supported Cu clusters (black) and the corresponding gas-phase Cu clusters (blue).
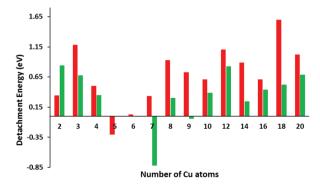

Fig. 3 Calculated detachment energies of a Cu atom from $CeO_2(111)$ supported Cu_n clusters (n = 2–10, 12, 14, 16, 18, and 20) with (green column) and without (red column) CO adsorption. Since the CO adsorption on Cu_5 and Cu_6 results in a spontaneous dissociation of clusters to form a Cu_1–CO complex nearby on $CeO_2(111)$, the detachment energies in the presence of CO are not included.

small clusters. For Cu_2, for example, the detachment energy is as low as 0.34 eV. By adding a Cu to form Cu_3, this value significantly increased to 1.18 eV. The lowest detachment energy is found for the Cu_5 cluster with a value of −0.3 eV, suggesting that a Cu atom might be facilely separated from the cluster. For n equal to 6–10, the detachment energies are moderate. While for n larger than 10, the detachment energy becomes larger. The detachment energy is determined by the balance between the interaction energy of the detaching Cu with the rest of the Cu cluster and with the $CeO_2(111)$ surface. We also calculated the detachment energies as the elementary reaction step between Cu_n and Cu_{n-1} + Cu_1, where the Cu atom is placed in the most favorable adjacent site away from its original position in the Cu_{n-1} cluster. The results are listed in Table S3.†

Based on these calculated detachment energies, it can be concluded that atomic detachment for Cu clusters on $CeO_2(111)$ is not impossible but very difficult. High temperatures are necessary. The generally endothermic detachment also suggests exothermic reattachment of Cu atoms to another cluster. In addition, some of the clusters might be more stable than others.

3.2 Influence of CO adsorption on Cu detachment from $CeO_2(111)$

In order to understand the effect of a molecular adsorbate on the detachment of a single Cu atom from a Cu cluster on ceria, we first examined the adsorption of a single CO molecule on Cu clusters on $CeO_2(111)$. Fig. 1(c) shows the Cu_n clusters (n = 2–10, 12, 14, 16, 18, and 20) on $CeO_2(111)$ with a single CO adsorption on a corner Cu atom. For all the clusters, the calculated C–O bond length is about 1.16 Å, which is 0.02 Å longer than that in its gas phase, and the C–Cu bond is 1.81 Å on average. However, the distances from the Cu atom with the CO adsorption to other adjacent Cu atoms typically increase. However, the shapes of all the clusters are not significantly changed in the presence of CO.

Detachment energies for Cu clusters on $CeO_2(111)$ with a single CO adsorption are compared with those for the same supported Cu clusters without CO. As seen in Fig. 3 (green columns), the adsorption of CO exclusively lowers the detachment energy, except for Cu_2. The amount of energy saving, which is quite significant, differs with the cluster size. For Cu_7 and Cu_9, for example, we can see that the detachment energy is significantly reduced from 0.33 and 0.72 eV for bare clusters to −0.82 and −0.04 eV in the presence of CO, respectively. This observation suggests that the adsorption of a single CO generally helps in the detachment. Interestingly, the CO adsorption on the 2D Cu_5 and Cu_6 clusters results in a spontaneous dissociation of clusters to form a Cu_1–CO complex nearby on $CeO_2(111)$. Such spontaneous formation of carbonyl species containing single metal (Au) atoms from oxide supported metal clusters has been reported before in AIMD studies.[65,66] Nonetheless, most detachment processes are endothermic, and thus still require high temperatures. The detachment energies in the elementary reaction step between Cu_n–CO and

Cu_{n-1} + Cu_1–CO, where the Cu_1–CO complex is adsorbed in the most stable adjacent site away from its original position in the Cu_{n-1} cluster, are also evaluated. When this method is used, the adsorption energy is also included for Cu detachment with CO. In this case, the detachment energies for the spontaneous detachment of Cu_5 and Cu_6 can be obtained. All the calculated data can be seen in Table S3.†

Similar results have also been observed on the Pd and Au clusters on ceria.[30,34] For Pd clusters on ceria, it is found that CO adsorption can reduce the detachment energy for Pd_n (n = 5–20) clusters due to the larger adsorption energy (−2.40 eV) of CO on a detached single Pd atom.[34] For Au clusters on ceria, it is observed from AIMD simulation that an isolated Au atom spontaneously attaches to a Au NP in the absence of CO, while Au_1–CO is quite stable at the ceria surface.[32] This trend can readily be understood as CO is a strong adsorbate. On a single Cu atom on $CeO_2(111)$, CO has a larger adsorption energy of −2.26 eV. As shown in Table S1,† the adsorption energies of CO on the supported Cu clusters are also quite significant, in the range of −1.50 – −0.50 eV. The lower detachment energy is partly due to the weaker adsorption of CO. For example, a small adsorption energy (−0.50 eV) of CO on Cu_7 indeed leads to a low detachment energy of −0.82 eV. We also evaluated different adsorption sites for CO. The result shows that a CO can be adsorbed on the top layer of Cu_7 and the co-adsorption of another CO on the bottom layer is not sterically hindered with a larger binding energy of −0.93 eV. In addition, the adsorption of CO thus weakens the Cu–Cu bonds in the cluster. For example, for Cu_{14}, the distances between the detached Cu and two closest Cu atoms are changed from 2.39 and 2.53 Å to 2.64 and 2.65 Å after CO adsorption.

It should be noted that the result depends on the structure and adsorption configuration of the Cu_n cluster on CeO_2 and on the CO adsorption site on the Cu_n clusters. However, the qualitative conclusions are not affected. To demonstrate this point, various cluster adsorption configurations and CO adsorption sites are tested for Cu_8 as an example. Indeed, as shown in Table S4,† different adsorption states lead to different binding energies. For each configuration of Cu_8, two CO adsorption sites are considered (Fig. S3†), and the corresponding detachment energies were obtained. We can see from Table S4† that these values also depend on the initial adsorption configurations of Cu_8. However, the calculated ΔE, the difference between $E_{det}(CO)$ and $E_{det}(no\ CO)$, is in the range of −0.50 to −1.17 eV, confirming that the adsorption of CO on Cu can significantly reduce its detachment energy and help in the formation of single atom species on $CeO_2(111)$.

We also investigated the effect of CO coverage on the energy cost for detaching a Cu atom from $CeO_2(111)$ supported Cu clusters. It can be seen in Fig. 4 that the detachment process for Cu_8 becomes less endothermic with the reaction energy changing from 0.30 to 0.11 eV when the number of adsorbed CO species is increased from 1 (low coverage) to 7 (high coverage). For Cu_8 on $CeO_2(111)$ without CO adsorption, the distances between the detaching Cu and three nearby Cu atoms in the cluster are calculated to be 2.52, 2.43, and 2.60 Å. For

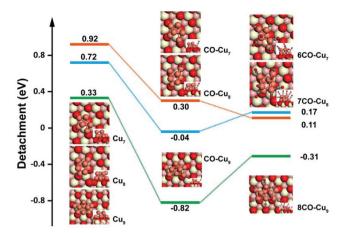**Fig. 4** Calculated detachment energies of a Cu atom from $CeO_2(111)$ supported Cu_n ($n = 7-9$) with $(CO)_m$ ($m = 0$, 1, and 7) adsorption. Color scheme: Ce, yellow; surface O, red; subsurface O, coral; Cu, bronze; C, grey.

only one CO adsorption on Cu_8, these values are found to be 2.66, 2.50, and 2.81 Å. While for seven CO adsorption on Cu_8, these values changed to 2.64, 2.55 and 2.84 Å, indicating that the interaction between the detached Cu and the nearby Cu atoms is weakened by the increasing CO coverage. This trend is consistent with the argument that the CO adsorption helps in the detachment of a single Cu from the Cu cluster by weakening the Cu–Cu bonds in the cluster. The average binding energy of CO is about −1.00 eV, indicating the possibility of the existence of high coverage of CO.

We also tried to evaluate the effect of high CO coverage on the energy cost for detaching a Cu atom from other clusters on $CeO_2(111)$. However, since the optimization of these structures with high CO coverage results in very high computation costs, only two other medium-sized clusters of Cu_7 and Cu_9 are explored. From the calculation results, the high coverage of 6 CO adsorbed on Cu_7 significantly reduces the detachment energy from 0.33 eV in the absence of CO to −0.31 eV. For 8 CO adsorbed on Cu_9, the detachment energy is about 0.17 eV, which is 0.55 eV lower than that without CO. It should be noted from Fig. 4 that the detachment energies for Cu_7 and Cu_9 under high coverage are more positive than that in the presence of only one CO, different from the case of Cu_8. Based on these results, we conclude that CO adsorption helps in the reduction of the energy cost for detaching a Cu atom from the $CeO_2(111)$ supported Cu clusters but the effect of CO coverage is still unclear. Further calculations for the effect of CO coverage on various Cu clusters will be carried out in future work.

The aforementioned theoretical results strongly suggest that the presence of CO helps in the detachment of atomic Cu from Cu clusters on ceria. The energetic information provided by these DFT calculations is still insufficient to provide a quantitative gauge on the enhancement. This is because the sizes of the Cu clusters studied here are still too small to cover the much larger (~nm) size clusters in real catalysts. In addition, extensive kinetic simulations based on NEB and *ab initio* mole-

cular dynamics (AIMD) calculations are needed to compare with the experiment. Nonetheless, the role of CO adsorption in atomic detachment is clearly established.

3.3 Migration of the Cu atom and Cu_1–CO complex on ceria

Ostwald ripening includes not only the detachment of single metal atoms from and attachment to NPs but also the migration of the single atom species between the two. Here, we examine the diffusion barriers of both a single Cu atom and the Cu_1–CO complex on $CeO_2(111)$. As shown in Table 1, the binding energy for the atomic Cu to $CeO_2(111)$ at the oxygen hollow site (Fig. 5a) without CO adsorption is −2.55 eV. This is consistent with the experimental value of ~−2.32 eV.[67] The Cu–O bond distances are 2.03, 2.03 and 2.07 Å. From the NEB calculation (Fig. 6), the activation barrier for the diffusion of a single Cu atom from this most stable site to an adjacent oxygen hollow site (see Fig. S4†) is 0.95 eV (Fig. 6). Another migration pathway is also considered from the hollow site to an adjacent oxygen top site, yielding a larger energy barrier of 1.06 eV. These results suggest that the migration of atomic Cu on $CeO_2(111)$ is quite difficult, in contrast to low diffusion barriers for the Pd (0.14 eV)[34] or Au (0.26 eV)[30] atom on $CeO_2(111)$. The reason might be that the radius (1.28 pm) of the Cu atom is relatively smaller and the atom is connected to three O atoms at the oxygen hollow site with a large binding

Table 1 Binding energies of the single Cu atom and the Cu_1–CO complex on adsorption on $CeO_2(111)$ and CeO_2 step as well as key structural parameters. The structures can be seen in Fig. 5

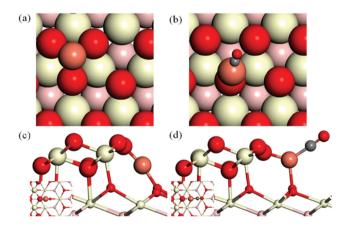| Species	Site	Binding energy (eV)	d_{Cu-O} (Å)	d_{Cu-C} (Å)
Cu	111	−2.55	2.03, 2.03, 2.07	—
	Step	−3.92	1.82, 1.83	—
Cu_1–CO	111	−3.05	1.77	1.77
	Step	−3.55	1.91, 2.04	1.80

Fig. 5 Optimized structures of a single Cu atom (a and c) and Cu_1–CO complex (b and d) adsorption on $CeO_2(111)$ and a CeO_2 step. Color scheme: Ce, yellow; surface O, red; subsurface O, coral; Cu, bronze; C, grey.
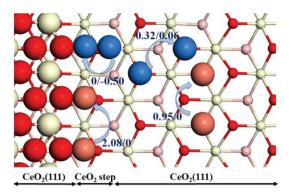
Fig. 6 The diagram for the migration of a single Cu atom on CeO$_2$(111) and at a CeO$_2$ step as well as the diffusion of the Cu$_1$–CO complex on CeO$_2$(111) with energy barriers/reaction energies (eV). Color scheme: Ce, yellow; surface O, red; subsurface O, coral; Cu, bronze; Cu$_1$–CO complex, blue. The corresponding structural information and the CI-NEB minimal energy paths for these processes are shown in Fig. S4–S6.†

energy of −2.55 eV and an average Cu–O bond length of 2.04 Å. While in the case of Au, the radius (1.44 pm) of the Au atom is much larger than that of the Cu atom, leading to a preferred adsorption configuration at the bridge site between two surface O atoms. The adsorption energy of the Au atom is calculated to be −1.18 eV, and the Au–O bond distance is about 2.18 Å.[68] Au can readily migrate from the preferred site to the other site, which was confirmed by another DFT work.[32]

Interestingly, the CO adsorption helps in the migration process of a single Cu atom on CeO$_2$(111). In Fig. 5b, it is shown that the Cu$_1$–CO complex prefers to adsorb on top of a surface oxygen with a tilted angle and the Cu–O distance is found to be 1.77 Å. It has a comparable binding energy (−3.05 eV) to atomic Cu, but the diffusion of the complex to an adjacent oxygen top site on CeO$_2$(111) is very facile with a low energy barrier of merely 0.32 eV (see Fig. 6). This result is in sharp contrast to the high barrier (0.80 eV) reported for the diffusion of the Au–CO species on CeO$_2$(111).[16]

3.4 Trapping at step sites

We further investigate the possibility of forming a stable single Cu species on ceria. It is well known that ceria surfaces, even the (111) face, contain a large number of defects.[69] As reported in the previous studies, single Pt and Au atoms may be stabilized by the ceria surface defects such as steps.[32,39] For example, Dvorak *et al.* showed that single Pt atoms can bind strongly on ceria, most likely at the step edges.[41] In this work, we investigate the possibility of trapping Cu or the Cu$_1$–CO complex on a unique step site of ceria.[32,39] To this end, a low-energy monolayer (ML) high step was selected as the slab model with the edge oriented along the [1$\bar{1}$0] direction of CeO$_2$. The adsorption geometry of the Cu or Cu–CO species at the step site is shown in Fig. 5c and d. For the single Cu atom, the binding energy is calculated to be −3.92 eV with Cu–O distances of 1.82 and 1.83 Å. It is important to note that the

binding energy is larger than the calculated cohesive energy of bulk Cu (−3.69 eV) and those for smaller clusters (Fig. 2). For the Cu$_1$–CO complex, on the other hand, the adsorption energy is slightly smaller with a value of −3.55 eV, and the bond lengths of Cu–O are equal to 1.91 and 2.04 Å. The strength of binding is still quite strong. The calculated binding energy of CO on the Cu SAC is about −0.62 eV, indicating that CO can facilely desorb from the Cu SAC. Such a single-atom species is expected to resist sintering, even at very high temperatures.

Furthermore, the diffusion process of the Cu$_1$–CO complex from a terrace site to the step site is explored (Fig. 6). This process was found to be spontaneous. On the other hand, the Cu atom at the step site is quite stable, and the calculated barrier is 2.08 eV. The corresponding structural information for these processes is shown in Fig. S5.†

The Cu atom on the step can probably serve as a SAC for some reactions. Here, the oxygen reduction reaction (ORR) is selected as a probe reaction to evaluate its potential catalytic applications. The calculation details are shown in the ESI.† As displayed in Fig. S7,† the calculated overpotential of the ORR on the Cu–CeO$_2$ SAC is about 0.70 V, very close to the lower limit of 0.69 V for commercial Pt/C (0.69–1.68 V).[70,71] Therefore, the CeO$_2$ supported Cu SAC might be a potential catalyst for the ORR. Further work will be carried out to explore other possible reactions on this Cu SAC.

4. Conclusions

In this work, we examined the atomistic mechanism of the Ostwald ripening of CeO$_2$(111) supported Cu$_n$ (n = 2–10, 12, 14, 16, 18, and 20) by DFT calculations. Our theoretical results found that the adsorption of CO on Cu clusters not only facilitates the detachment of a Cu atom from the Cu cluster onto the CeO$_2$(111) surface but also lowers the energy barrier for the diffusion of a single Cu species on CeO$_2$(111). These observations suggest that the presence of CO can greatly facilitate disintegration of Cu clusters and atomic redispersion on ceria. This is largely made possible by the strong CO adsorption on Cu, which weakens the Cu–Cu bonding in the clusters. Although the sintering kinetics is not simulated in this work, the exploration of the energy landscape for the key steps of Ostwald ripening provides the first step toward a better understanding of the atomistic mechanism of this important process in catalysis.

The possibility of detachment and diffusion of single-atom species of Cu on CeO$_2$(111) also allows the exploration of the formation of possible SACs. Our theoretical results suggest that the CeO$_2$ step edge is a possible site for the location of the Cu$_1$–CO complex, generating a stable single Cu motif that resists sintering. Moreover, we also demonstrate that the CeO$_2$ supported Cu SAC might be a potential catalyst for the ORR due to a low overpotential. This work provides important physical insights for the design of efficient heterogeneous catalysts, especially the single atom catalysts.

Conflicts of interest

There are no conflicts to declare.

Acknowledgements

References

1 G. V. Sagar, P. V. R. Rao, C. S. S. And and K. V. R. Chary, *J. Phys. Chem. B*, 2006, **110**, 13881.

2 J. A. Rodriguez, P. Liu, J. Hrbek, J. Evans and M. Perez, *Angew. Chem., Int. Ed.*, 2007, **46**, 1329–1332.

3 M. Behrens, F. Studt, I. Kasatkin, S. Kühl, M. Hävecker, F. Abild-Pedersen, S. Zander, F. Girgsdies, P. Kurr and B. L. Kniep, *Science*, 2012, **336**, 893–897.

4 J. Paier, C. Penschke and J. Sauer, *Chem. Rev.*, 2013, **113**, 3949–3985.

5 Y. Zhu, X. Kong, D. Cao, J. Cui, Y. Zhu and Y. Li, *ACS Catal.*, 2014, **4**, 3675–3681.

6 J. Graciani, K. Mudiyanselage, F. Xu, A. Baber, J. Evans, S. Senanayake, D. Stacchiola, P. Liu, J. Hrbek and J. Fernández Sanz, *Science*, 2014, **345**, 546–550.

7 P. Munnik, P. E. de Jongh and K. P. de Jong, *Chem. Rev.*, 2015, **115**, 6687–6718.

8 B. Yang, C. Liu, A. Halder, E. C. Tyo, A. B. F. Martinson, S. Seifert, P. Zapol, L. A. Curtiss and S. Vajda, *J. Phys. Chem. C*, 2017, **121**, 10406–10412.

9 J. A. Rodríguez, J. Evans, J. Graciani, J.-B. Park, P. Liu, J. Hrbek and J. F. Sanz, *J. Phys. Chem. C*, 2009, **113**, 7364–7370.

10 K. Mudiyanselage, S. D. Senanayake, L. Feria, S. Kundu, A. E. Baber, J. Graciani, A. B. Vidal, S. Agnoli, J. Evans, R. Chang, S. Axnanda, Z. Liu, J. F. Sanz, P. Liu, J. A. Rodriguez and D. J. Stacchiola, *Angew. Chem., Int. Ed.*, 2013, **52**, 5101–5105.

11 M. V. Twigg and M. S. Spencer, *Appl. Catal., A*, 2001, **212**, 161–174.

12 M. Kurtz, H. Wilmer, T. Genger, O. Hinrichsen and M. Muhler, *Catal. Lett.*, 2003, **86**, 77–80.

13 R. V. D. Berg, T. E. Parmentier, C. F. Elkjær, C. J. Gommes, J. Sehested, S. Helveg, P. E. D. Jongh and K. P. D. Jong, *ACS Catal.*, 2015, **5**, 4439–4448.

14 P. J. F. Harris, *Int. Mater. Rev.*, 1995, **40**, 97–115.

15 E. D. Goodman, J. A. Schwalbe and M. Cargnello, *ACS Catal.*, 2017, **7**, 7156–7173.

16 S. Wanke and P. Flynn, *Catal. Rev.*, 2012, **12**, 93–135.

17 T. W. Hansen, A. T. Delariva, S. R. Challa and A. K. Datye, *Acc. Chem. Res.*, 2013, **46**, 1720–1730.

18 P. Wynblatt and N. A. Gjostein, *Acta Metall.*, 1976, **24**, 1165–1174.

19 C. T. Campbell, S. C. Parker and D. E. Starr, *Science*, 2002, **298**, 811–814.

20 S. C. Parker and C. T. Campbell, *Phys. Rev. B*, 2007, **75**, 035430.

21 A. T. DeLaRiva, T. W. Hansen, S. R. Challa and A. K. Datye, *J. Catal.*, 2013, **308**, 291–305.

22 F. Solymosi and M. Pasztor, *J. Phys. Chem.*, 1985, **89**, 4789–4793.

23 A. Suzuki, Y. Inada, A. Yamaguchi, T. Chihara, M. Yuasa, M. Nomura and Y. Iwasawa, *Angew. Chem., Int. Ed.*, 2003, **42**, 4795–4799.

24 S. B. Simonsen, I. Chorkendorff, S. Dahl, M. Skoglundh, J. Sehested and S. Helveg, *J. Am. Chem. Soc.*, 2010, **132**, 7968–7975.

25 G. S. Parkinson, Z. Novotny, G. Argentero, M. Schmid, J. Pavelec, R. Kosak, P. Blaha and U. Diebold, *Nat. Mater.*, 2013, **12**, 724.

26 R. Addou, T. P. Senftle, N. O'Connor, M. J. Janik, A. C. T. van Duin and M. Batzill, *ACS Nano*, 2014, **8**, 6321–6333.

27 R. Bliem, J. E. van der Hoeven, J. Hulva, J. Pavelec, O. Gamba, P. E. de Jongh, M. Schmid, P. Blaha, U. Diebold and G. S. Parkinson, *Proc. Natl. Acad. Sci. U. S. A.*, 2016, **113**, 8921–8926.

28 R. Ouyang, J.-X. Liu and W.-X. Li, *J. Am. Chem. Soc.*, 2013, **135**, 1760–1771.

29 B. R. Goldsmith, E. D. Sanderson, R. Ouyang and W.-X. Li, *J. Phys. Chem. C*, 2014, **118**, 9588–9597.

30 Y. G. Wang, D. Mei, V. A. Glezakou, J. Li and R. Rousseau, *Nat. Commun.*, 2015, **6**, 6511.

31 P. N. Plessow and F. Abild-Pedersen, *ACS Catal.*, 2016, **6**, 7098–7108.

32 J. C. Liu, Y. G. Wang and J. Li, *J. Am. Chem. Soc.*, 2017, **139**, 6190–6199.

33 W. Janse van Rensburg, P. van Helden, D. J. Moodley, M. Claeys, M. A. Petersen and E. van Steen, *J. Phys. Chem. C*, 2017, **121**, 16739–16753.

34 Y. Q. Su, J. X. Liu, I. A. W. Filot and E. J. M. Hensen, *Chem. Mater.*, 2017, **29**, 9456–9462.

35 X. Wang, J. A. van Bokhoven and D. Palagin, *Phys. Chem. Chem. Phys.*, 2017, **19**, 30513–30519.

36 D. R. Mullins, *Surf. Sci. Rep.*, 2015, **70**, 42–85.

37 A. Bruix, Y. Lykhach, I. Matolínová, A. Neitzel, T. Skála, N. Tsud, M. Vorokhta, K. Ševčíková, J. Mysliveček, R. Fiala,

M. Václavů, K. C. Prince, S. Bruyère, V. Potin, F. Illas, V. Matolín, J. Libuda and K. M. Neyman, *Angew. Chem., Int. Ed.*, 2014, **53**, 10525–10530.

38 B. Qiao, J. Liu, Y. G. Wang, Q. Lin, X. Liu, A. Wang, J. Li, T. Zhang and J. Liu, *ACS Catal.*, 2015, **5**, 6249–6254.

39 J. Jones, H. Xiong, A. T. Delariva, E. J. Peterson, H. Pham, S. R. Challa, G. Qi, S. Oh, M. H. Wiebenga, X. I. Pereira Hernández, Y. Wang and A. K. Datye, *Science*, 2016, **353**, 150–154.

40 F. Li, L. Li, X. Liu, X. C. Zeng and Z. Chen, *ChemPhysChem*, 2016, **17**, 3170–3175.

41 F. Dvořák, M. F. Camellone, A. Tovt, N. D. Tran, F. R. Negreiros, M. Vorokhta, T. Skála, I. Matolínová, J. Mysliveček and V. Matolín, *Nat. Commun.*, 2016, **7**, 10801.

42 H. Xiong, S. Lin, J. Goetze, P. Pletcher, H. Guo, L. Kovarik, K. Artyushkova, B. M. Weckhuysen and A. K. Datye, *Angew. Chem., Int. Ed.*, 2017, **56**, 8986–8991.

43 L. Nie, D. Mei, H. Xiong, B. Peng, Z. Ren, H. Xip, A. Delariva, M. Wang, M. H. Engelhard, L. Kovarik, A. K. Datye and Y. Wang, *Science*, 2017, **358**, 1419.

44 X.-F. Yang, A. Wang, B. Qiao, J. Li, J. Liu and T. Zhang, *Acc. Chem. Res.*, 2013, **46**, 1740–1748.

45 A. Bruix, K. M. Neyman and F. Illas, *J. Phys. Chem. C*, 2010, **114**, 14202–14207.

46 A. Figueroba, G. Kovács, A. Bruix and K. M. Neyman, *Catal. Sci. Technol.*, 2016, **6**, 6806–6813.

47 Y. Tang, Y.-G. Wang and J. Li, *J. Phys. Chem. C*, 2017, **121**, 11281–11289.

48 Y. Wang, Z. Chen, P. Han, Y. Du, Z. Gu, X. Xu and G. Zheng, *ACS Catal.*, 2018, **8**, 7113–7119.

49 J. P. Perdew, J. A. Chevary, S. H. Vosko, K. A. Jackson, M. R. Pederson, D. J. Singh and C. Fiolhais, *Phys. Rev. B*, 1992, **46**, 6671–6687.

50 G. Kresse and J. Hafner, *Phys. Rev. B*, 1993, **47**, 558–561.

51 G. Kresse and J. Furthmüller, *Phys. Rev. B*, 1996, **54**, 11169–11186.

52 G. Kresse and J. Furthmüller, *Comput. Mater. Sci.*, 1996, **6**, 15–50.

53 G. Kresse and D. Joubert, *Phys. Rev. B*, 1999, **59**, 1758–1775.

54 M. Huang and S. Fabris, *J. Phys. Chem. C*, 2008, **112**, 8643–8648.

55 G. Henkelman and H. Jónsson, *J. Chem. Phys.*, 2000, **113**, 9978–9985.

56 G. Henkelman, B. P. Uberuaga and H. Jónsson, *J. Chem. Phys.*, 2000, **113**, 9901–9904.

57 E. Şakir and R. Shaltaf, *Phys. Rev. A*, 1999, **60**, 3053–3057.

58 K. Jug, B. Zimmermann, P. Calaminici and A. M. Köster, *J. Chem. Phys.*, 2002, **116**, 4497–4507.

59 P. Jaque and A. Toro-Labbé, *J. Chem. Phys.*, 2002, **117**, 3208–3218.

60 J. Wang, G. Wang and J. Zhao, *Chem. Phys. Lett.*, 2003, **380**, 716–720.

61 E. M. Fernández, J. M. Soler, I. L. Garzón and L. C. Balbás, *Phys. Rev. B*, 2004, **70**, 165403.

62 H. Grönbeck and P. Broqvist, *Phys. Rev. B*, 2005, **71**, 073408.

63 G. H. Guvelioglu, P. Ma, X. He, R. C. Forrey and H. Cheng, *Phys. Rev. Lett.*, 2005, **94**, 026103.

64 C. Kittel, *Am. J. Phys.*, 2005, **21**, 547–548.

65 Y.-G. Wang, Y. Yoon, V.-A. Glezakou, J. Li and R. Rousseau, *J. Am. Chem. Soc.*, 2013, **135**, 10673–10683.

66 Y.-G. Wang, D. C. Cantu, M.-S. Lee, J. Li, V.-A. Glezakou and R. Rousseau, *J. Am. Chem. Soc.*, 2016, **138**, 10467–10476.

67 T. E. James, S. L. Hemmingson and C. T. Campbell, *ACS Catal.*, 2015, **5**, 5673–5678.

68 M. F. Camellone and S. Fabris, *J. Am. Chem. Soc.*, 2009, **131**, 10473–10483.

69 Z. Wu, M. Li, D. R. Mullins and S. H. Overbury, *ACS Catal.*, 2012, **2**, 2224–2234.

70 J. K. Nørskov, J. Rossmeisl, A. Logadottir, L. Lindqvist, J. R. Kitchin, T. Bligaard and H. Jónsson, *J. Phys. Chem. B*, 2004, **108**, 17886–17892.

71 D.-H. Lim and J. Wilcox, *J. Phys. Chem. C*, 2012, **116**, 3653–3660.